第 54 卷第 4 期
2026 年 4 月

硅 酸 盐 学 报
JOURNAL OF THE CHINESE CERAMIC SOCIETY

Vol. 54，No. 4
April，2026

http://jccsoc.cbpt.cnki.net

DOI：10.14062/j.issn.0454-5648.20250637

综 合 评 述

韩国应用型玻璃研究的最新进展

YOON Il Jung[1], LEE Jae sung[2], JUNG In-Ho[2,3], CHUNG Woon Jin[4], CHO Jung-Wook[5], CHOI Yong Gyu[1]

(1. 韩国航空大学材料科学与工程系，高阳市 10540，韩国；2. 首尔国立大学材料科学与工程系，首尔市 08826，韩国；3. 首尔国立大学先进材料研究所，首尔市 08826，韩国；4. 公州国立大学先进材料工程学部，天安市 31080，韩国；5. 浦项科技大学钢铁与生态材料技术研究生院，浦项市 37673，韩国)

摘　要：韩国的下游玻璃产业与其他非亚洲国家存在显著区别，其半导体和显示面板产业与玻璃材料供应链的关联更为紧密。本文介绍了这类应用的 2 个典型案例，即用于柔性智能手机盖板的超薄玻璃，以及用于高性能半导体封装的玻璃核心基板与玻璃中介层。上述特定应用需要配套的尖端功能玻璃后处理技术，这类技术的研发主要由产业界与学术界合作推动。本文聚焦韩国高校主导开展的、与玻璃材料直接或间接相关的应用型研究工作，引入了 4 个不同的研究方向：1) 玻璃形成体系的热力学数据库；2) 铸钢用保护渣体系；3) 掺杂量子点和/或钙钛矿纳米晶体的玻璃；4) 用于热成像的硫系玻璃。针对每个研究方向，本文均结合其基本概念与未来发展前景，阐述了相关领域的最新研究进展。

关键词：超薄玻璃；玻璃芯基板；CALPHAD 热力学数据库；保护渣；量子点与钙钛矿玻璃；硫系玻璃
中图分类号：J527.3　　**文献标志码**：A　　**文章编号**：0454–5648(2026)04–1340–19
网络出版时间：2026–01–23

1 Introduction

The semiconductor and display industries of South Korea are quite competitive compared to those of other countries. These two industry sectors normally require glass materials as core and/or auxiliary components in their manufacturing processes. In the case of glass materials employed in such high-tech industries, producing high-quality pristine glasses needs to precede all other steps in order to meet the overall quality standards of final products; however, it is sometimes more critical to better perform post-treatments of the pristine glasses for desired shape and/or functionality. Here, the distinct features of glass-related research and development in South Korea are delineated by taking two representative applications of glasses. The first example concerns glass for use in semiconductor packaging applications: not only glass core substrates but also glass interposers containing large amounts of through-glass vias (TGVs) are attracting unprecedented attention for their employment in semiconductor packaging. Glass-based substrates and interposers offer exceptional flatness and thermal stability, enabling finer circuit patterning and higher wiring density. This is supposed to lead to up to 40% faster data processing speeds and over 40% lower power consumption compared to silicon or polymeric substrates, thus allowing for next-generation chip stacking and advanced lithography that enable artificial

收稿日期：2025–08–29。　修订日期：2025–10–27。
基金项目：Material and Parts Research and Development Project (RS-2024-00441443) funded by the Ministry of Trade, Industry & Energy (MOTIE, Korea); Materials Technology Development Program (RS-2024-00450608) funded by the Ministry of Trade, Industry & Energy (MOTIE, Korea)。
第一作者：YOON Il Jung (1997—)，女，博士研究生。
通信作者：JUNG In Ho (1972—)，男，博士，教授；
CHUNG Woon Jin (1972—)，男，博士，教授；
CHO Jung Wook (1965—)，男，博士，教授；
CHOI Yong Gyu (1968—)，男，博士，教授。

Received date: 2025–08–29.　**Revised date:** 2025–10–27.
First author: YOON Il Jung (1997–), female, Doctoral candidate.
E-mail: ij970521@gmail.com
Correspondent author: JUNG In Ho (1972–), male, Ph.D., Professor;
CHUNG Woon Jin (1972–), male, Ph.D., Professor;
CHO Jung Wook (1965–), male, Ph.D., Professor;
CHOI Yong Gyu (1968–), male, Ph.D., Professor.
E-mail: in-ho.jung@snu.ac.kr; wjin@kongju.ac.kr; jungwook@postech.ac.kr; ygchoi@kau.ac.kr

intelligence and high-performance computing [1]. Taking into consideration the inherent brittleness of glass, care should be paid to each unit process from laser irradiation and subsequent chemical etching to singulation. This reasoning supports the view that the relevant technologies are actively driven by industry together with academia in South Korea, largely based on experience acquired during processing glasses for flexible OLED display as well as large-area flat panel display. The second example is ultra-thin glass (UTG) for use as a cover window of a flexible display panel. In an attempt to endow sodium alumino-silicate glass with the flexibility needed for foldable smartphones, UTGs with thickness of ~30 μm are typically used. This thickness is expected to increase for better robustness and visual appearance in the folding region. In this case, all the relevant processes including cutting, polishing, chamfering, etching and chemical strengthening should be performed with extra care [2]. Flexible display devices with other form factors featuring multi-foldable, slidable or rollable capability would be enabled along with advancement of processing technologies associated with UTG.

On the other hand, South Korean scientists and engineers involved in glass research are dealing with various properties and functionalities of glass materials like those in other countries. In this review article, the authors intend to concentrate on research activities mainly led by Korean academia rather than by Korean industry or national institutes. This review prioritizes subtopics more closely relevant to industrial applications of glass rather than fundamental scientific aspects of glass from among the wide range of research topics being performed by Korean universities. In the course of surveying candidate subtopics that properly satisfy the strategy poised in this review, the authors came to realize that certain research activities would be worth highlighting: to assist ceramic materials design and pyrometallurgical production technology development, basic phase diagram study and thermodynamic database development have been carried out in collaboration with academic partners and industrial partners. Fundamental studies on glass forming and polymeric structuring behaviors of multi-oxide silicate systems have been mostly carried out in conjunction with the steelmaking industry in an attempt to enhance both the productivity and quality of steel products. In addition, studies on glasses with optical functionalities have been focused more on the glasses containing quantum dots or nanocrystals for color converts as well as the chalcogenide glasses for thermal imaging lens assemblies. Taking into consideration the above-mentioned activities, the authors present representative progresses, which are not necessarily the best results, performed in South Korean universities with an emphasis on applications of glass. Four different subtopics are covered: 1) a thermodynamic database for glass-forming systems; 2) mold flux systems used in steel casting; 3) glasses doped with quantum dots and/or perovskite nano-crystals; 4) chalcogenide glasses for thermal imaging. It should be noted that other research topics directly or indirectly related to glass are actively pursued by South Korean researchers.

2 Development of a thermodynamic database for the applications to glasses

2.1 CALPHAD methodology

Recently thermodynamic calculations using accurate and comprehensive thermodynamic databases are frequently applied in materials science and engineering fields. A thermodynamic database is developed through the CALculation of PHAse Diagram (CALPHAD) methodology [3–4]. The schematic representation of thermodynamic optimization (modeling) based on the CALPHAD approach is shown in Fig. 1. In CALPHAD modeling, the Gibbs energies of all phases in a target system are assessed consistently based on all available data. For example, the Gibbs energy of a stoichiometric compound is simply described as a function of temperature and pressure. The Gibbs energy of a solution phase can vary with composition as well. Therefore, selecting a proper thermodynamic model that reflects the structure of the solution is an important prerequisite. The model parameters for the Gibbs energy function can be optimized based on all available thermodynamic property data and overall phase equilibrium data involving the given phase. When the Gibbs energy functions of all phases in a target system are obtained, any type of

thermodynamic calculations such as phase diagrams, complex chemical reactions involving solid, liquid and gas phases, and evolution of enthalpy with process, *etc*. can be performed to understand the materials synthesis and processing within a system. The thermodynamic model can make the prediction of phase equilibria and chemical reactions of higher order systems from the model parameters optimized in lower order systems.

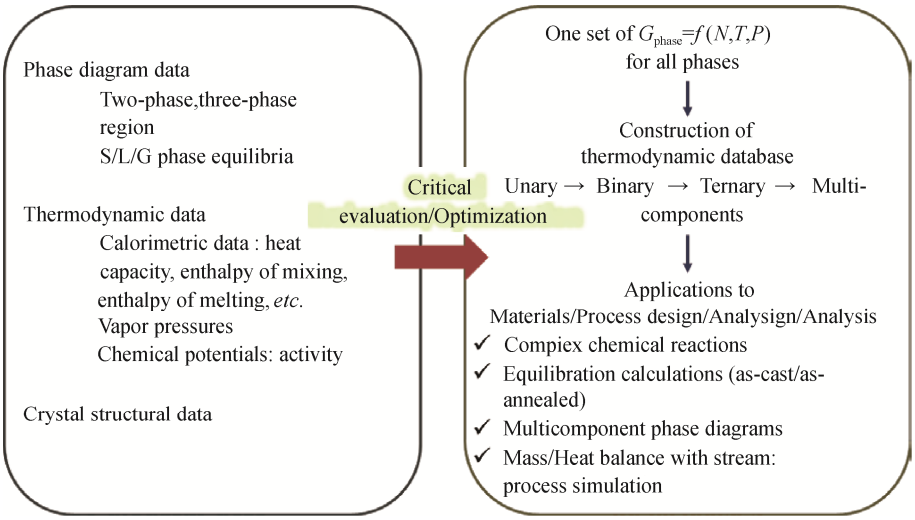

Fig. 1 Schematic representation of the CALPHAD thermodynamic database development procedure

FactSage (www.factsage.com) and ThermoCalc (www.thermocalc.com) are two thermodynamic software packages that are the most frequently accessed for industrial applications of pyrometallurgy, glassmaking, ceramics, *etc*. Other thermodynamic software packages like MTDATA (National Physical Laboratory, UL), and MPE (CSIRO, Australia) are also used for pyrometallurgical processes. The applications of thermodynamic software packages to steelmaking and pyrometallurgical processes have been reviewed several times [5–7].

2.2 FactSage software and thermodynamic database

The accuracy of thermodynamic calculations of multicomponent phase diagrams and phase equilibria depend highly upon the algorithm that minimizes the total Gibbs energy of a system with a set of constraints and the availability of an accurate and comprehensive thermodynamic database relevant to the target application systems. The FactSage software employs the powerful ChemSage algorithm [7] for Gibbs energy minimization, which allows for complex thermodynamic calculations involving up to 40 elements, 200 solutions, and 1500 stoichiometric compounds per equilibration calculation. This ChemSage routine allows elemental inputs down to 10^{-61} mol and calculates results down to a cutoff limit of 10^{-75} mol. Therefore, FactSage is optimal to perform equilibrium calculations for material processes that require high precision such as a high-purity fused quartz production requiring ppb to ppm level of impurity concentration calculations.

The FactSage databases [6–8] contain the most comprehensive collection of critically evaluated and optimized data for inorganic systems. In CALPHAD modeling, a selection of appropriate thermodynamic models for each solution phase is critical for a large and reliable thermodynamic database with a high predictive capability. In order to accurately describe the entropy of solution, the solution model should reflect the solution structure. In particular, the FactSage thermodynamic databases adopt the Modified Quasichemical Model (MQM) [9–10] to describe complex liquid solutions like molten oxide (slag or glass), molten sulfides, molten salts, and liquid metallic solutions. The MQM considers the short-range ordering of the second-nearest neighbors of cations in a liquid oxide solution. For example, MQM can consider the well-known silicate network breaking reaction occurring in a molten oxide solution. The Compound Energy Formalism [11] is also used as a framework for solid solutions having multi-sublattice structures for ions and atoms. The examples for solid solutions are well described in the previous study [11].

2.3 Recent thermodynamic database development

Professor In-Ho Jung's research group at Seoul National University (SNU) is one of the key developer groups of the FactSage thermodynamic database. In particular, the FACT oxide database (FTOxid) and steel database (FSStel) which have a wide range of applications in steelmaking, glassmaking, cements, engineering ceramics, non-ferrous production, etc. have been largely developed by Prof. Jung's research group. FTOxid database (version 8.4) contains 553 stoichiometric solids, 112 multi-component solid solutions such as spinel, pyroxenes, melilite, olivine, monoxide, etc., and liquid solution within SiO_2-Li_2O-Na_2O-K_2O-CaO-MgO-Al_2O_3-FeO_x-MnO-TiO_x-CrO_x-SnO_x-ZrO_2-NiO-CoO-P_2O_5-Cu_2O-As_2O_3-GeO_2-PbO-ZnO-RE_2O_3 system. For liquid oxide solution, a dilute solubility of S, SO_4, PO_4, H_2O/OH, CO_3, F, I, and Cl can also be computed. The FTOxid database can be directly applied to complex chemical reactions in various stages of glass production including batching, melting (batch-to-melt conversion), fining (refining), forming, and annealing.

Recent glass and special ceramics related databases constructed by Prof. In-Ho Jung's group include (1) a ZrO_2 containing system [10–11]: CaO-MgO-Al_2O_3-SiO_2-Na_2O-FeO-MnO-ZrO_2; (2) a Sn oxide containing system [12-14]: CaO-MgO-Al_2O_3-SiO_2-Na_2O-SnO-SnO_2; and (3) a soda glass and LAS (Li_2O-Al_2O_3-SiO_2) glass based system [15–16]: Na_2O-K_2O-Li_2O-CaO-MgO-Al_2O_3-SiO_2.

Unfortunately, many glass systems often lack phase diagram and thermodynamic property data in the related literature, which makes accurate thermodynamic database development challenging. In this case, phase diagram experiments are often conducted to support thermod- ynamic modeling and database development. The phase diagram experiments for glass systems can be conducted using the classical equilibration/ quenching method and differential scanning calorimetry/differential thermal analysis followed by X-ray diffraction (XRD) and electron probe micro analysis (EPMA) for phase determination and compositional analysis, respectively. In the experiment, special attention should be paid to 1) the choice of suitable crucible materials to prevent the contamination of the sample, 2) managing volatility of components [13, 19] like Na_2O, K_2O, Li_2O, P_2O_5 and B_2O_3, and 3) prevention of hydration of hygroscopic materials [13, 20] like K_2O, Li_2O and Na_2O. In addition, compositional analysis of components such as Li_2O, Na_2O, and B_2O_3 is difficult in EPMA. Thus, compositional analyses of components like B_2O_3 and Na_2O must be conducted by employing a large beam diameter, low current, and low voltage conditions [13, 21].

Fig. 2 shows the complex phase diagrams calculated from the established thermodynamic database. The phase diagram of the spodumene ($LiAlSi_2O_6$)-enstatite ($MgSiO_3$)[17] is shown in Fig. 2a, which can be used to predict the

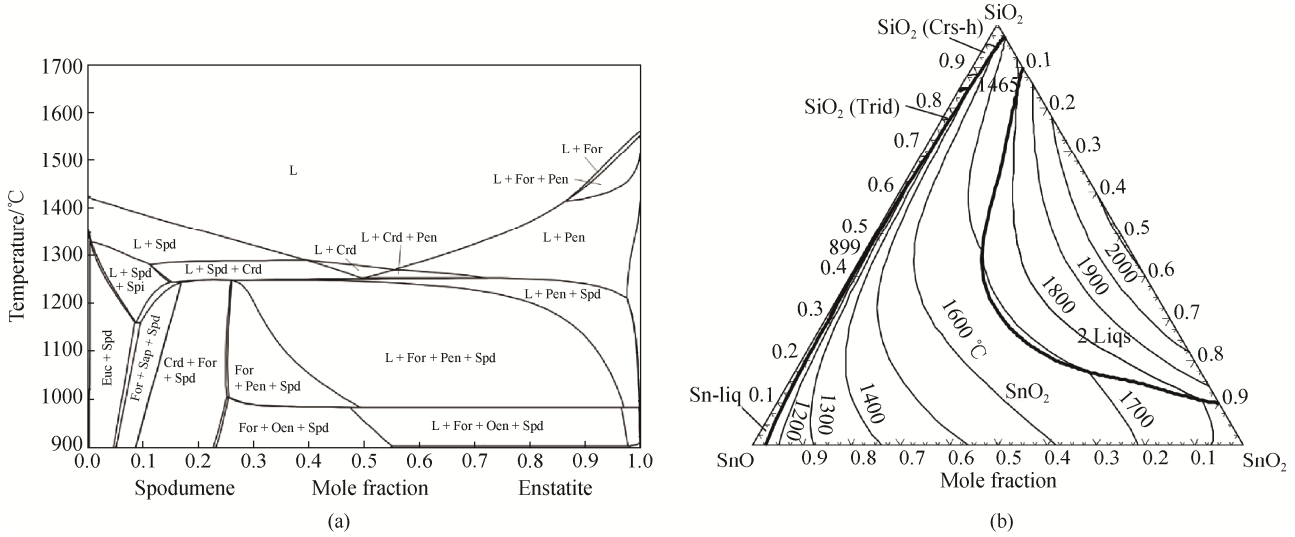

Crd: Cordierite; Euc: Eucryptite; For: Forsterite; L: Liquid; Oen: Ortho-enstatite; Pen: Proto-enstatite; Sap: Sapphire; Spd: Spodumene.

Fig. 2　Calculated (a) phase diagram of the spodumene-enstatite system [18] and (b) liquidus projection [16] of the SnO-SnO_2-SiO_2 system

phase stability of LAS-based glass ceramics under compositional modifications by MgO or $MgSiO_3$. The liquidus projection of the SnO-SnO_2-SiO_2 system [14] presented in Fig. 2b is a fundamental system to understand the chemical reactions between Sn bath and glass occurring in the float bath process.

2.4 On-going research for glass applications

The thermodynamic database can be applied to phase equilibrium prediction, redox control, and process optimization in the glass making process (Fig. 3). For example, in the float bath where liquid Sn is used to flatten glass and make a thin glass ribbon, undesired evaporation of Sn and chemical reaction between liquid Sn and glass ribbon can occur. In this process, forming gas [N_2 with 5%–10% (in volume fraction) H_2] is flushed to prevent the oxidation of Sn and chemical reaction with glass. The oxygen partial pressure of forming gas is controlled by the dew point management (–10 ℃ to –30 ℃). In the float bath, Sn and various Sn—O gas species can be produced in the hot temperature zone of the float bath by evaporation and condense under oxidizing conditions in the low temperature zone which potentially induces defects on glass. In a recent study by Lee *et al.* [14], thermodynamic calculations were carried out to understand the evaporation of liquid Sn and condensation of Sn and SnO_2 from gas in the float bath.

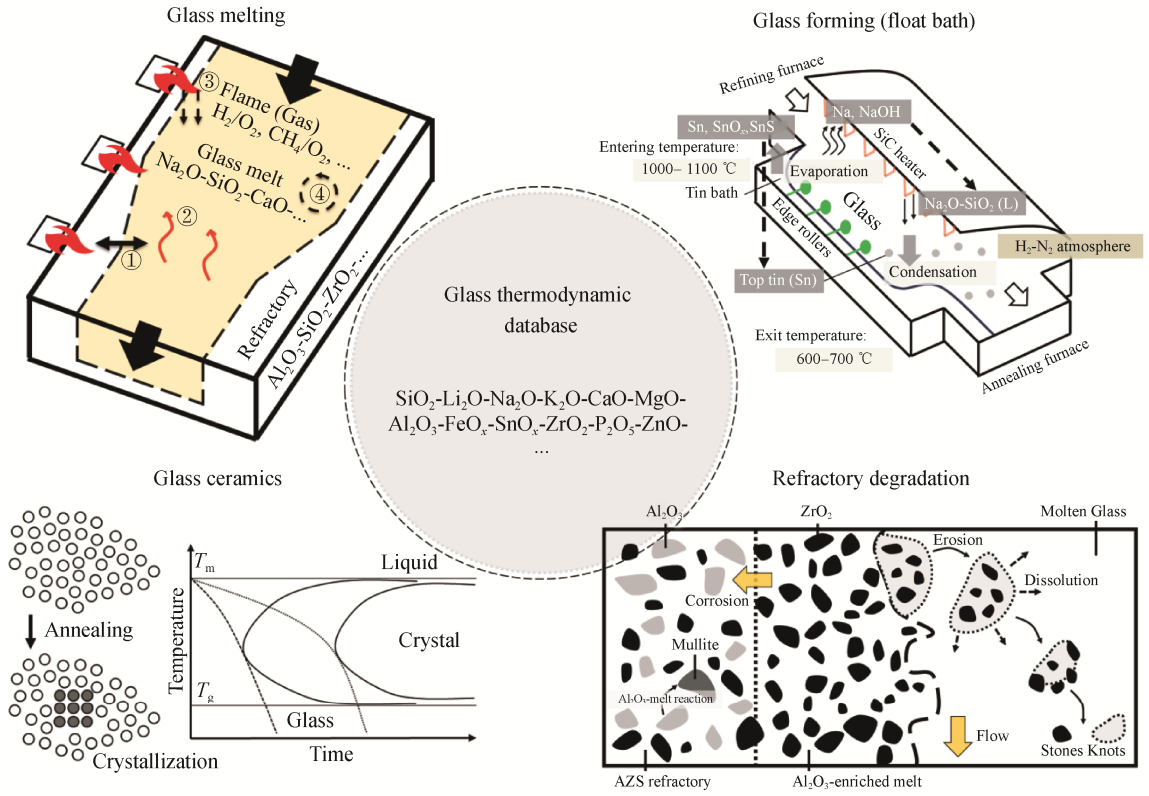

Fig. 3 Applications of thermodynamic database to glass making processes

In order to reduce CO_2 emission, more H_2 burners will be employed in a glass melting furnace. As a result, the gas environment in glass melting furnace will be changed from CO–CO_2–H_2O gas to H_2–H_2O gas. Under H_2–H_2O gas environment, glass can uptake a certain amount of H_2O (in liquid glass melt, it is dissolved in the form of OH^- and H_2O). Therefore, the solubility of H_2O in glass depending on temperature and glass composition is important to understand H_2O bubble formation. The redox control to prevent such H_2O bubble formation is a new research topic. New thermodynamic databases are being developed to address these H_2O related issues [22].

To understand the refractory wear in the furnace, thermodynamic analysis is essential. In particular, AZS type refractory is frequently used in glass production. The degradation of refractory can be significantly influenced by the impurity level in AZS refractory. To understand this, the phase diagram and viscosity data of liquid glass

are important. Research on this mechanism is in progress, specifically by combining thermodynamic and viscosity calculations [23–25].

Development of new glass ceramics by changing the additive to LAS glass is another long term research topic. In order to understand how various additives such as SnO_2, TiO_2, P_2O_5, MgO, *etc*. influence the nucleation kinetics of eucryptite and spodumene, phase diagram study of the eucryptite-additive systems and the spodumene-additive systems has been conducted extensively. Phase diagram data, such as the solubility of such additives to eucryptite and spodumene phases and selective crystallization of certain nucleus phases, can help in designing the assisted nucleation process of eucryptite and spodumene.

Diffusion of oxide components in glass is important for simulation of precipitation kinetics and growth of crystals in glass and dissolution of refractory materials in glass. Recently, a diffusion model for liquid silicate system was developed by Kwon *et al*. [26–27] and the diffusivity of oxide component in molten oxide is under investigation using liquid diffusion couple experiments.

3 Glass lubricants applied for continuous casting of steels

The continuous casting of steel is an unavoidable process which transforms molten metal into a solid as a step in the production of metallic materials. Presently, more than 95% of commercial steel products are being produced *via* continuous casting. In the continuous casting of steel, mold flux plays the most important and unique role to guarantee both the successful operation and the high quality of products. As the mold flux is a kind of multi-component lubricant glass which infiltrates into the gap between a solid steel shell and a copper mold to prevent sticking, achieving excellent lubrication at the mold wall is critical. The lubrication capacity of glass is closely relevant to viscosity and solidification temperature. At the same time, controlling mold heat transfer through its crystallinity is another important function of mold flux. Mold heat flux density should be maintained under a threshold value at the vicinity of the meniscus to avoid surface cracks on cast steel products. The mechanism by which the crystallinity of the mold flux controls heat transfer can be suggested as increase of interfacial thermal resistance due to volumetric contraction, increase of radiative thermal resistance due to larger absorption coefficient, and increase of conductive thermal resistance due to voids. Because the crystalline deteriorates the lubrication of the mold slag film, there should be limitations on the amount of crystalline in the slag film so as not to incur serious surface defects on cast steels.

In order to satisfy the two important roles above, the commercial mold flux largely consists of SiO_2 as the principal network former, and other network modifiers CaO, Na_2O, and CaF_2. Aside from the major quaternary system, several minor components such as Al_2O_3, MgO, and B_2O_3 would be included. It should be emphasized that the mold flux will have a film-like shape in a continuous casting mold in which the film will further be separated into liquid or supercooled liquid phase on the higher temperature steel shell side, and solid glass or glass-ceramic phase on the lower temperature copper mold side. As mentioned above, in order to control the mold heat flux below the critical level, the solid phase should contain the optimum amount of crystal of cuspidine, $Ca_4Si_2O_7F_2$.

3.1 Viscoelastic behavior of SiO_2-based glass lubrication melts

During continuous casting operations, as can be seen from Fig. 4, the mold flux fed into the casting mold melts to form the liquid slag pool on the mold top surface. Then, the liquid slag is drawn down into the gap along the steel shell and lubricates the strand to form the slag film which consists of a partially crystalline solid layer and a fully liquid layer. Thus, the liquid slag film layer is sandwiched between a solid steel shell and a crystalline flux layer. This liquid slag film causes lubrication, preventing the steel shell from adhering to the mold. In doing so, the liquid slag film helps to prevent surface cracks in the steel or a breakout in which molten steel bursts out of the shell. To meet an optimum casting condition, the exact viscosity value of mold flux itself is important. In order to understand the dynamic lubrication in an oscillating casting mold, the rheological behavior of the mold flux at different shear rates has been investigated in consideration of structural characteristics of liquid and/or supercooled liquids of

various mold flux systems [28-33]. One of the important challenges to overcome is to design mold flux systems with a proper value of viscosity. This is because the viscosity of the mold flux has to be large enough at the mold top surface (10 – 40 cm^{-1}) in order to alleviate slag entrainment and low enough at the mold wall (100 – 1000 cm^{-1}) for maximizing lubricating capability, as shown in Table 1. Therefore, the non-Newtonian behavior of shear thinning characteristic would be highly beneficial to enhance the performance of mold flux at both the positions (Fig. 4). This being the case, investigation of the shear-thinning behavior of molten mold flux glassy state has been conducted using a rotational viscometer, for conventional CaO-SiO_2-Na_2O-CaF_2 [28, 32], and a new series of CaO-CaF_2-SiO_2-Si_3N_4 [29, 30, 32], CaO-CaF_2-SiO_2-B_2O_3 [31–32], and CaO-CaF_2-SiO_2-SiC [33]. The Ostwald De Waele power law model has been adopted to express the flow curve of shear stress to shear rate.

$$\eta = K(\dot{\gamma})^{n-1} \quad (1)$$

where K is consistency, n is flow behavior index, η is viscosity, and $\dot{\gamma}$ is viscosity. The flow behavior index, n is a dimensionless number that relates the closeness to Newtonian flow. When the amount of n is in between 0 and 1, the fluid is called shear thinning. All the glass systems investigated showed shear thinning behavior with lower flow behavior index than 1; 0.87–0.93 for CaO-SiO_2-Na_2O-CaF_2 [28], 0.84–0.92 for CaO-CaF_2-SiO_2-B_2O_3 [31], 0.81–0.88 for CaO-CaF_2-SiO_2-Si_3N_4 [29], and 0.78–0.82 for CaO-CaF_2-SiO_2-SiC [33] systems, respectively. Generally, a larger degree of polymerization induces a smaller flow behavior index. However, it is noteworthy from those investigations that a generation of an overly stiff structure of the calcium silicate melts causes an increase on the flow behavior index indicating that the melt loses its shear thinning property [30, 33].

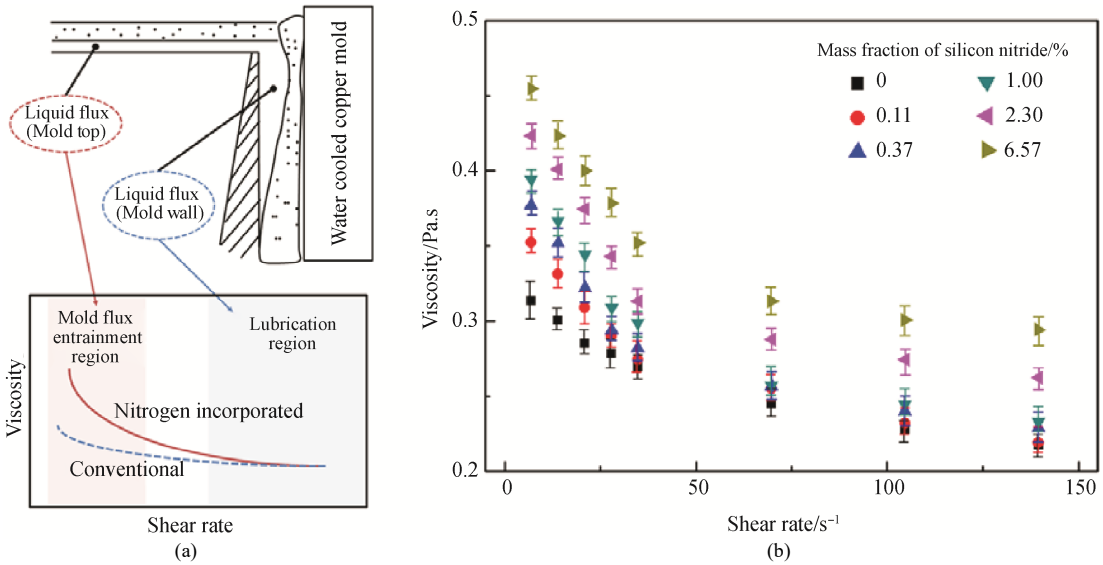

Fig. 4 (a) Schematic of a continuous casting mold showing glassy mold flux layer on top surface and at the mold, and (b) viscoelastic behavior of Si_3N_4 containing mold flux system [30]

Table 1 Estimated shear rate in liquid mold flux during continuous casting operation

Position	Thickness of liquid mold flux/(10^{-3}m)	Maximum relative velocity in the liquid flux layer/(m·s^{-1})	Maximum shear rate /s^{-1}
Mold top surface	5.0–10.0	0.10–0.20	10–40
Mold wall	0.2–0.5	0.05–0.20	100–1000

3.2 MAE (mixed alkali effect) of mold flux glasses

In order to meet the demands of higher casting speeds for better productivity, Li_2O has generally been added into conventional quaternary mold flux systems. It is believed that the role of Li_2O should be controlling the nucleation kinetics of cuspidine moderately, but the mechanism has not been clarified. Investigations on isothermal and non-isothermal crystallization kinetics of cuspidine in CaO-SiO_2-Na_2O-Li_2O-CaF_2 mold flux system showed that the obvious delay of cuspidine nucleation happens by addition of Li_2O [34–36]. Therefore, larger basicity (CaO/SiO_2) with Li_2O addition could be

regarded as an effective countermeasure to enhance both the lubrication and controlling heat transfer by dispersion of tiny cuspidine crystal particles into mold flux film at mold wall during high-speed casting of steels, which aligns with commercial production experiences [35].

However, still there are two possibilities for the mechanism for delayed nucleation by Li_2O. The first is in cooperation of direct Li-F bonding in molten state [34, 36] suggested from 7Li, 19F MAS NMR and molecular dynamics simulations. Also, the MAE (Mixed Alkali Effect) is believed to be the origin of nucleation retardation. Investigations have been done on MAE of various potential mold flux glass systems by mixing Li_2O, Na_2O, and K_2O together, using Raman and NMR spectroscopies. Then, it has been suggested that a new characteristic of MAE, an increase in charge compensation stability of a small alkali when mixed with a larger cation, should be beneficial for stabilizing the glass forming ability of $CaO\text{-}SiO_2\text{-}Al_2O_3\text{-}CaF_2$ system with various alkali cations even at higher temperatures [37]. The systematical assessments on MAE have been followed for $CaO\text{-}SiO_2\text{-}CaF_2\text{-}B_2O_3$ quaternary system by addition of Na and Li cations [38], for phosphate glass by mixing Na and Li cations [39], and for simple alkali borate ternary glasses systems [40]. The results indicate a general model of MAE for various kinds of glass systems, shown in Fig. 5, where the well-known site-mismatch model at lower temperature than T_g (glass transition temperature) and matrix-mediated coupling model at around T_g are included. Furthermore, the understanding of MAE could be enlarged into supercooled liquids by employing the multiple relaxation processes model at even higher than T_g [40]. Based on this model, the application of MAE could be expanded to various kinds of mold fluxes to enhance the glass forming ability of silicate, alumino-silicate, and alumino-borosilicate mold flux systems. Also, controlling the crystallization kinetics and morphology of crystalline could be achieved by application of MAE, even at a lower cost without the addition of Li_2O.

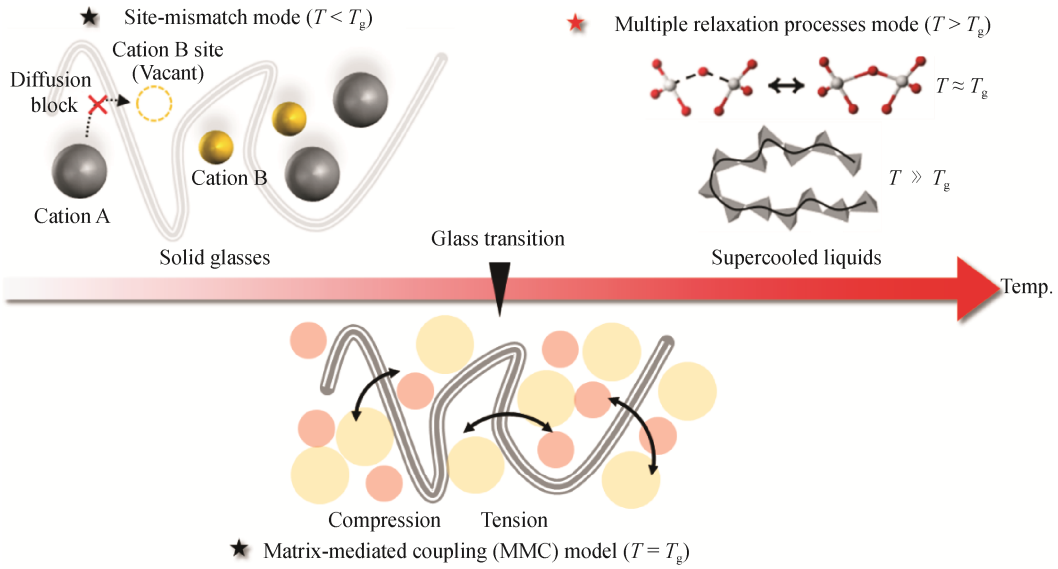

Fig. 5　Suggested mechanism for MAE (mixed alkali effect) at various temperatures

3.3　Metallic particle dispersion in mold flux glasses

The function of conventional mold flux of quaternary $CaO\text{-}SiO_2\text{-}Na_2O\text{-}CaF_2$ can be optimized comparatively easily by controlling the morphology and size of cuspidine crystalline. However, the demands for green and eco-friendly steel production processes force the removal of fluorine or the addition of larger amounts of Al_2O_3 in commercial mold flux systems, where the primary cuspidine crystallization cannot happen [41–42]. Various attempts have been performed on the development of alternative crystalline phases but have yet to succeed. From this point, our investigations were motivated to develop a novel technology to control heat transfer without worsening the lubrication with unwanted crystalline phases.

Investigations have been carried out to clarify the

effect of tiny metallic iron particles of controlled size distribution, 0.5–3.0 μm to enhance the Mie scattering, on the radiative heat transfer through mold flux [43–45]. The extinction coefficients of iron particles decreased considerably, from 733 m^{-1} to 4415 m^{-1} by addition of 1% (in mass fraction) of iron particles into $CaO\text{-}SiO_2\text{-}Na_2O\text{-}B_2O_3$ glassy mold flux system, as shown in Fig. 6. Further investigations using a pilot scale tester showed that overall heat flux density through mold flux with metallic particles, in consideration of both conduction and radiation simultaneously, can be reduced by more than 50% [45]. This performance has been supported by thermal conductivity of metallic particles containing mold flux [46]. Overall, thermal boundary resistance has been generated at the interface between metallic particle and matrix glass, which in turn reduces both the radiative and conductive thermal conductivity by scattering [46]. The new glass lubricants with a small amount of metallic particles should be responsible for clean and green steel manufacturing processes by removing environmentally detrimental components such as fluorine.

Sample	SiO_2	CaO	MgO	Al_2O_3	Na_2O	F	B_2O_3	Fe*
A	33.7	33.8	0.9	4.4	6.4	6	14.8	0
B	32.4	32.3	0.9	4.2	6.1	5.8	14.2	0.5
C	31.0	31.1	0.8	4.1	5.9	5.5	13.6	0.8
D	30.3	30.4	0.8	4.0	5.8	5.4	13.3	1.0

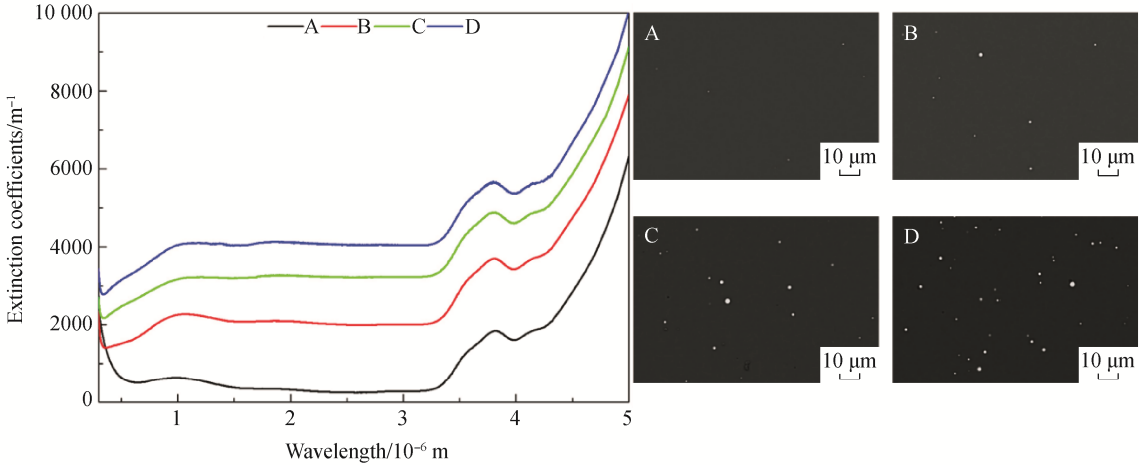

Fig. 6 Extinction coefficient of glassy mold fluxes as a function of wavelength with the micrographs showing the presence of iron metallic particles [45]

4 Quantum dots and nanocrystal embedded glasses for LED color conversion

White light emitting diodes (wLEDs) are widely used as a common light source for various applications such as display, lighting, and automobile headlamps. Conventional wLEDs consist of an InGaN based blue LED chip and phosphors as color converters. The phosphors are mixed with silicone resin to be pasted on top of the blue LED in conventional wLEDs. However, the inherent chemical and thermal instability of resin hinder their application to high power applications, bringing in complete inorganic color converters made from glass materials. Phosphor-in-glass (PiG) which embeds ceramic phosphors with transparent glasses via sintering, has emerged as a robust solution for color conversion in high-power solid-state lighting, offering superior thermal and chemical stability compared to conventional resin-based converters [47]. The first report on PiG involved Pb-free silicate glass for a white LED color converter (Fig. 7a) [48], which enabled the commercial application of PiG as an automobile headlamp. Although PiG provides practical solutions for robust color conversion, it requires additional sintering processes and the use of separate crystalline ceramic phosphor materials. Moreover, wLEDs for display applications require narrow emission bandwidths to achieve a wide color gamut and high picture quality, such as ultra-high definition (UHD) display. Quantum dots (QDs) are well-suited for this purpose, providing narrow emission bandwidths with high

conversion efficiency. However, chemically synthesized QDs suffer from their inherently weak chemical, thermal and photonic stability. Embedding quantum dots or nanocrystals in glasses as activators presents a promising alternative, offering a practical solution for various applications without the need for additional processing or separate phosphor materials. As a result, this approach has been extensively investigated, including fluoride nano-crystal embedded glasses, quantum dot embedded glasses and perovskite nanocrystal embedded glasses.

4.1 Fluoride nano-crystal embedded glasses

Oxyfluoride glass and glass-ceramics have been considered as promising inorganic color converters due to their hybrid characteristics of oxide matrices and embedded fluoride nanocrystals, which offer both chemical durability and low phonon environments to the doped active ions, respectively. Through systematic strategies on glass composition, nano-crystals and rare-earth dopants, emission properties mostly for the visible range under UV and blue LED excitation have been optimized. Early studies highlighted the rare-earth dependent formation of β-PbF_2 and LaF_3 nanocrystals, where Dy^{3+} showed enhancement in radiative emission intensity under 365 nm excitation [49–50]. Dual-valence control of Eu ions (Eu^{2+}/Eu^{3+}) in LaF_3-based matrices was also shown to enable white emission with adjustable coordinates under 400 nm LED excitation [51]. The formation of LaF_3 nanocrystals within SiO_2-Na_2O-Al_2O_3-based glass matrices effectively enhanced visible emissions of Dy^{3+} and Ho^{3+} under 455 nm excitation, with new green emissions attributed to phonon energy changes at the Dy^{3+} site [52]. Similarly, co-doping Eu^{2+} and Mn^{2+} enabled efficient white emission under 400 nm UV-LED, benefiting from energy transfer and complementary red emission from Mn^{2+} [53]. The incorporation of Eu^{2+} into a LaF_3-nepheline dual-phase system produced strong yellow emission and high photoluminescence quantum yield (PL-QY) up to 78% (Fig. 7b), demonstrating the feasibility for packaged UV-LED color conversion [54]. Pr^{3+}-doped glass-ceramics exhibited narrowband green and red emissions under 450 nm excitation, achieving wide color gamut values over 120% of the NTSC (National Television System Committee) defined area, suitable for display backlights [55]. Co-doping Eu^{3+}, Tb^{3+}, and Tm^{3+} ions into a BaF_2-Al_2O_3-B_2O_3-SiO_2 matrix yielded white light with pure chromaticity (x = 0.33, y = 0.33), a CRI of 91, and a QY exceeding 90%, aided by the formation of BaF_2 nanocrystals [56].

4.2 Quantum dot embedded glasses

Quantum dot embedded glasses (QDEGs) can offer a practical solution for stable and color-tunable phosphors in white LEDs by overcoming the inherent weakness of colloidal quantum dots (cQDs). Successful demonstration of CdSe and CdS embedded glasses as a color converter for blue LED was reported for the first time by Han *et al.* [57]. However, CdSe and CdS QDEG could not compose a white LED due to their limited PL-QY. White LED has been successfully fabricated by synthesizing CdSe/CdS core–shell structured Cd-S-Se QDEG, which exhibited significantly enhanced emission intensity thanks to the passivation of CdSe core [58] as shown in Fig. 7c. It clearly demonstrated the feasibility of QDEGs as a robust color converter for white LED with highly improved thermal and chemical stability compared to cQDs. QY of the Cd-S-Se QDEG has been improved up to 25% *via* optimization of glass composition and heat treatment conditions [59]. Rare-earths further doped the Cd–S–Se QDEG to adjust emission intensity and chromaticity via energy transfer and structural modification of rare earth ions within the glass matrix [60]. The formation mechanisms of CdSe/CdS QDs within oxide glass matrix was elucidated by studying excitonic absorption peak wavelength and Raman analysis, suggesting the initial crystallization of CdSe core QDs followed by the growth of CdS shell via the Oswald ripening process [61]. In order to use the Cd-S-Se QDEG in display applications, two Cd-S-Se QDEGs having green and red emission peak wavelengths were prepared in a sandwich structure to give dual emission and a broader color gamut [62].

4.3 Perovskite nanocrystal embedded glasses

Although QDEGs have demonstrated their potential as white LED color converters, their inferior PL-QY and emission bandwidth compared to commercial ceramic phosphors and cQDs hindered their practical applications. $CsPbX_3$ (X=Cl, Br and I) based perovskite nano-crystals (PNCs), however, have defect tolerance and do not

require passivation shells, allowing high PL-QY even in oxide glasses. Perovskite nanocrystal embedded glasses (PNEGs), thus guaranteeing thermal, chemical and photonic stability from which colloidal PNCs suffered, allow various applications as reviewed recently [63]. Regarding PNEG, recent research interest has focused mostly on the further improvement of PL-QY as well as stability employing additional passivation layers or finding new glass matrix. Double encapsulation of $CsPbBr_3$ perovskite nanocrystals in a PiG structure using a transparent silicate glass greatly improved stability, enabling a white LED with up to 131% NTSC color gamut using a combination of $CsPbBr_3$ and $K_2SiF_6:Mn^{4+}$ red phosphor [64]. Further improvements were made by developing flexible remote phosphor devices with UTG substrates, achieving 130% NTSC coverage as depicted in Fig. 7d [65]. While previous studies used germanate glass as a matrix, the use of borosilicate glasses as host matrices offered enhanced chemical durability compared to germanate systems. These borosilicate-based PNEGs demonstrated significantly enhanced water stability compared to germanate glasses [66]. Incorporation of Al_2O_3 and Ga_2O_3 improved the PL-QY of the silicate $CsPbBr_3$ PNEG up to 68% [67] and additional doping of Pr_2O_3 achieved the PL-QY of the silicate PNEG up to 73% [68] as a green color converter. PNEGs for red emission with $CsPb(Br/I)_3$ were also studied to improve their PL-QY. Red-emitting $CsPb(Br/I)_3$ PNEGs embedded in germanate glasses achieved PL-QY up to 70.5% with wide color gamut up to 139% of the NTSC defined area, suitable for UHD display applications [69]. Silicate based $CsPb(Br/I)_3$ red PNEGs also achieved high PL-QY even up to ~ 80%, demonstrating a wide color gamut up to ~139% of the NTSC defined area. It should be noted that

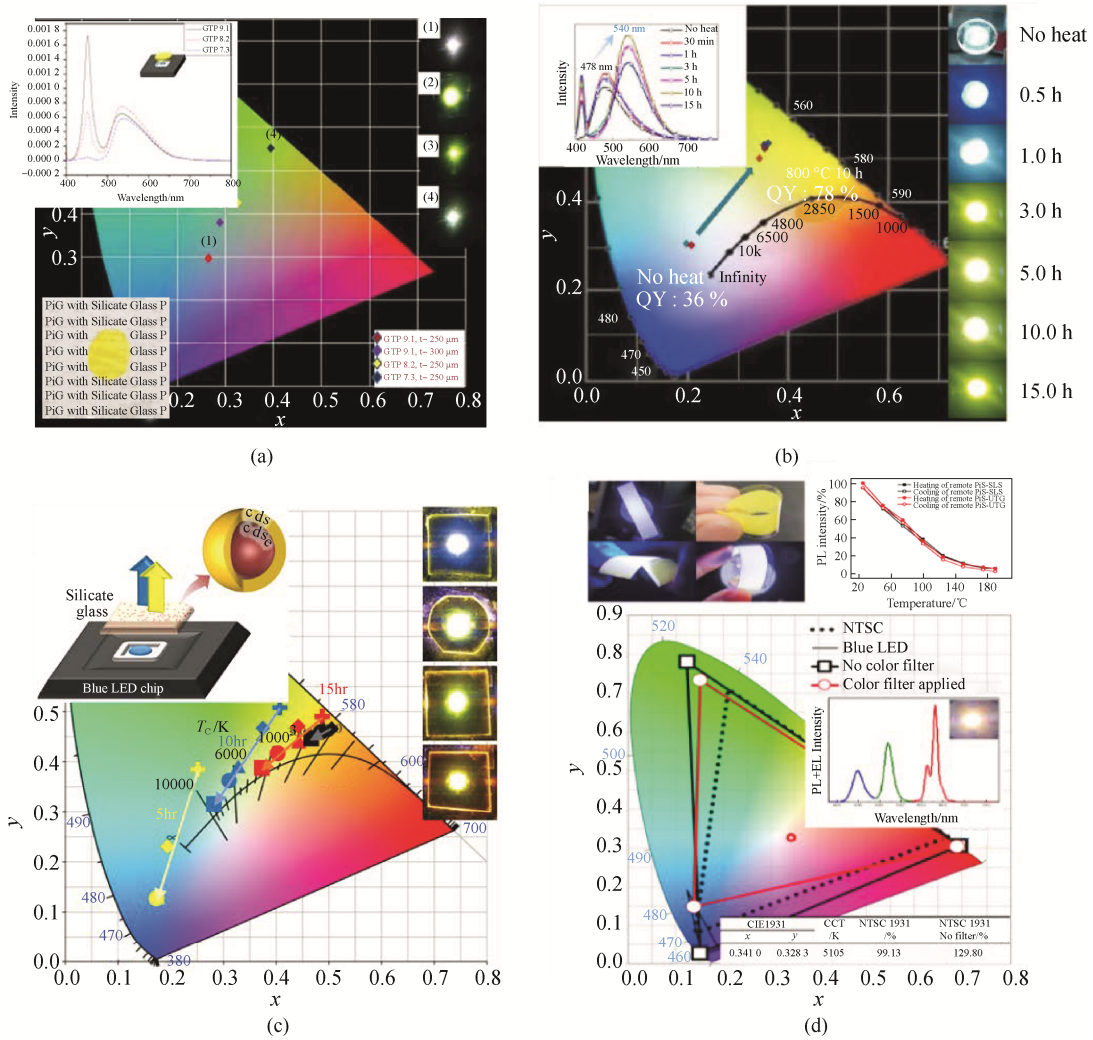

Fig. 7 (a) PiG with silicate glass [48], (b) Oxyfluoride glass ceramic with nepheline [54], (c) white LED with CdSe/CdS core-shell structured QDEG [58], and (d) flexible color converter with PNEG and UTG [65]

PL-QY above 70% for both green and red PNEGs are comparable to commercial phosphor ceramics or cQDs on the market proposing their practical feasibility as robust color converters for high picture quality display applications.

5 Chalcogenide glasses for thermal imaging

5.1 Why chalcogenide glasses for thermal-imaging applications

The longer-wavelength side of the optical transmission window of a pure dielectric continuum solid without electronic/vibrational impurities inside is normally governed by the multiphonon absorption of the representative and strongest vibrational mode. Typical oxide-based solids, either in the form of crystalline or glassy state, barely transmit up to ~7 μm due to their relatively higher representative phonon energy compared to that of non-oxide solids [70]. As such, thermal cameras that are capable of sensing photons in the long-wavelength infrared (LWIR; 8–12 μm) region and visualizing temperature distributions into two-dimensional images necessitate LWIR-transmitting dielectric materials. Since the capability of optical transmittance across the LWIR range is most prioritized for the refractive lens and/or protective windows, only some limited materials can be considered as good candidates. If imaging optics components realized via refraction (with partial assistance of diffraction in some cases) are our primary concerns, crystalline materials such as Ge, and Zn(S or Se) would effectively work as a lens assembly. However, it is well-known that these crystalline materials should be shaped into lenses using machining processes like diamond turning machining [71]. In particular, the significantly higher thermo-optic coefficient of single-crystalline Ge, stemming from its narrow bandgap energy [72] in addition to its higher density, needs to be taken into consideration when designing LWIR-imaging lens assembly. On the other hand, it is widely believed already that thermal imaging will soon be employed in automobiles in the form of advanced driver assistance systems (ADAS) [73]. In addition, the mandatory regulations relevant to the autonomous emergency braking (AEB) are set to come into effect in the coming years [74]. The proper operation of the AEB systems should rely on the use of thermal cameras under foggy and/or dimmed conditions. This trend raises a critical issue for the LWIR-imaging optics components: in short, the SWaP-C (size, weight and power consumption-cost) criteria should be applied when one needs to optically design a lens assembly working at the LWIR range. More specifically, lens materials and lens-forming processes should be devised to manufacture lens assembly that are more compact, lightweight, energy-efficient and cost-effective [75]. In order to minimize optical aberrations, use of multiple (more than doublet or triplet) lenses is needed. In this regard securing LWIR-transmitting materials in a wider range of refractive index and its dispersion, *i.e.*, expanding the LWIR Abbe diagram, should be pursued first [76].

The above reasoning validates the use of chalcogenide glass (ChG) as LWIR-imaging optics components. The compositional flexibility inherent to glass materials enables the commercialization of plural ChG compositions differing not only in refractive index at 10 μm but also in refractive index dispersion across the LWIR region. The viscous plastic deformation of ChGs at a proper temperature and pressure provides a unique opportunity for the precision glass molding (PGM) process into refractive lenses (sometimes with aspheric curvatures and/or diffractive optical elements).

5.2 Strategies for compositional tailoring of chalcogenide glasses

Performance as well as unit price of the uncooled microbolometer as an LWIR image sensor is rapidly improving to meet the demands of thermal cameras in the civilian sectors [77]. To keep up with such enhanced resolutions of LWIR image sensors, the corresponding lens assembly needs to be better functioning and more cost effective, which requires more abundant ChG compositions wide scattered in the LWIR Abbe diagram to achieve the “all-ChG-based lens assembly” compatible with thermal image sensors with VGA resolution or beyond (see the upper left panel in Fig. 8). Looking at the compositions of commercially available ChGs, one may observe that those compositions can be classified into two families, *i.e.*, Ge-based and As-based compositions [78]. It is well known that arsenic is the representative of hazardous materials, so that ChGs containing a large

amount of As would face greater difficulties during production and practical use (see the upper right panel in Fig. 8). Ge-based ChGs would be less hazardous; however, both the supply chain issue and the cost issue associated with high-purity Ge elements need to be resolved [79]. This suggests that ChGs containing less Ge or no Ge would be favored (see the lower left panel in Fig. 8). ChGs need to be compatible with molding processes to be better secured for mass production as shown in the lower right panel in Fig. 8.

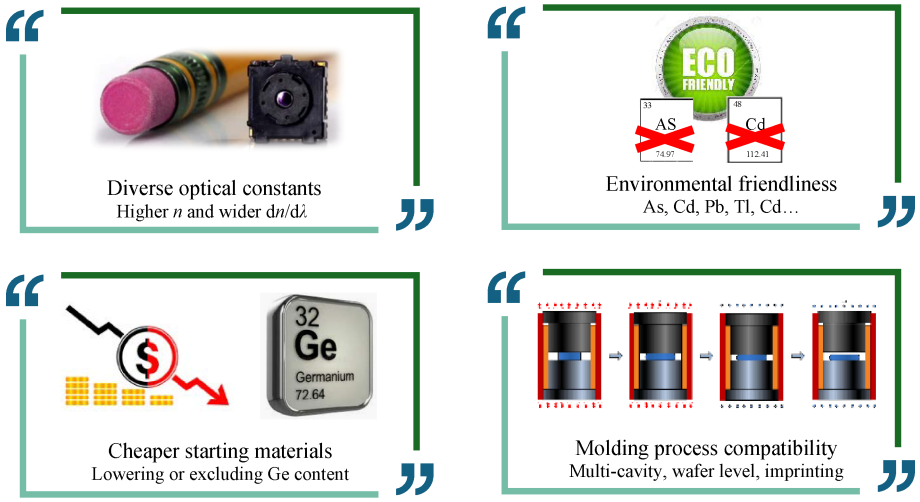

Fig. 8 Schematic diagram featuring possible research approaches in compositional search for chalcogenide glasses for use as LWIR-imaging applications: the four major criteria, *i.e.*, optical constants, toxicity, raw materials cost and molding compatibility, need to be taken into consideration in assessing feasibility of the existing and/or new chalcogenide glasses

Compositional searches for new ChG compositions based on unempirical or semi-empirical assessments would be beneficial in reducing trial and error. As the LWIR Abbe diagram shows, information on the wavelength dependence of refractive index is crucial to evaluate imaging performance. In an attempt to secure ChG compositions that can form highly dispersive glasses across the LWIR wavelengths, ternary Ge-Sb-S glasses were compositionally modified via addition of the fourth element, and then the accompanying effects on thermal, mechanical and optical properties were evaluated [80]. It was revealed in the case of quaternary Ge-Ga-Sb-S system that an increase in Sb content results in an increase in refractive index due to the high polarizability of Sb atom, whereas the relative amount of Sb to Ga exerts an insignificant effect on the refractive index dispersion in the LWIR range. Interestingly, the LWIR dispersion turned out to be more dependent on Ge content, which suggests that highly dispersive ChGs which are transparent across the LWIR range can be compositionally engineered using a Ge-Ga-Sb-S system. These findings exemplify that, by adjusting ChG compositions, it is possible not only to precisely control the infrared-side transmission edge, but also to numerically correlate the infrared-side transmission edge and the LWIR refractive index dispersion in a more straightforward manner [80]. As mentioned previously, the infrared-side transmission edge takes shape as a direct result of multiphonon absorption, so that the position of the infrared transmission edge has been interpreted qualitatively and crudely in terms of the bond energy of atomic pairs and molar mass of constituents. To derive a more facile model that correlates ChG compositions and their LWIR refractive index dispersion, Lee *et al.*[81] proposed the single average harmonic oscillator (SAHO) model capable of quantitative analysis of the compositional dependence of the infrared transmission edge. In this model, the infrared cutoff edge is assumed to be determined by a single harmonic oscillator corresponding to the average vibrational energy representing the overall vibrations of the covalently bonded ChG structure. Accordingly, the average bond energy (E_{ave}) and molar mass (M) are combined in combination in the SAHO model, both of which can be numerically available for any given ChG compositions [81]. By applying the SAHO model to Ge-based ChGs, it is shown that there is

agreement between predicted and experimental values of refractive index dispersion. Notably, Se-based ChG compositions with less dispersive refractive indexes and S-based ones with more dispersive refractive indexes were proposed with the aid of the present methodology. A doublet configuration consisting of these two ChG lenses experimentally demonstrated itself to be effective in decrease of chromatic aberrations across the LWIR range. Later, Lee *et al*. tried to apply the SAHO model to the mixed-chalcogen ChG system. As for the mixed-chalcogen Ge-Sb-Se-S glasses, it was verified that their infrared-side transmission edge tends to behave like sulfide glasses rather than selenide glasses [82]. Furthermore, Kim *et al*. [83] evaluated the universality of the SAHO model by studying a wide range of Ge-containing ChG systems, including sulfides, sulfo-selenides, selenides, seleno-tellurides, and tellurides (Fig. 9). Based on the results demonstrated using almost all subsets of Ge-based ChGs, it becomes more facile but more accurate at the same time in correlating the LWIR dispersion of ChGs and their chemical compositions [83]. Integration of newly found ChG compositions with engineered refractive index and/or dispersion, together with some commercially available compositions, into the LWIR Abbe diagram features a remarkable expansion to the higher refractive index but lower dispersion side, as displayed in Fig. 10 [84]. Again, the broadening of the LWIR Abbe diagram needs to be pursued for optical designs to better secure the all-ChG-based lens assembly with diverse functionalities in the LWIR spectral region.

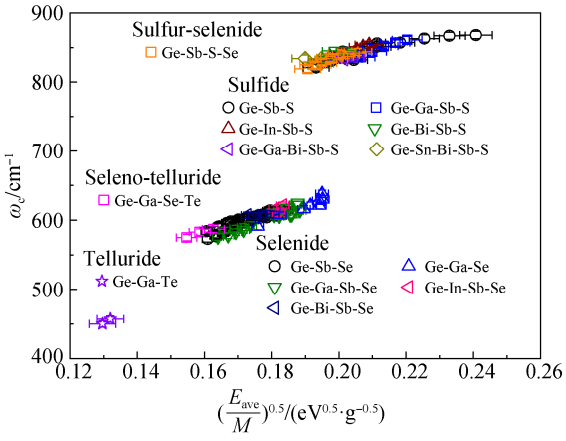

Fig. 9　Infrared transmission edge (ω_c) plotted as a function of SAHO parameter consisting of the average bond energy (E_{ave}) and molar mass (M) of any given compositions of Ge-based chalcogenide glasses [83]

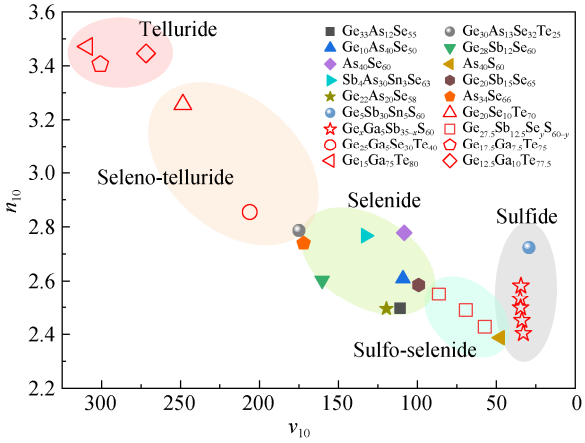

The closed symbols represent chalcogenide glasses readily commercialized, whereas the open symbols indicate new compositions proposed to further broaden the existing LWIR Abbe diagram [84]. Note that some of the new compositions are now commercially available as of 2025.

Fig. 10　An LWIR Abbe diagram composed of only chalcogenide glasses without crystalline materials

5.3　Assessment of molding process compatibility

To simultaneously achieve enhanced performance, miniaturization and cost reduction in the lens assembly of thermal camera applications, it is essential to adopt a comprehensive design strategy that encompasses not only optical characteristics but also moldability. During the molding process, the ChG must remain thermally stable without any noticeable crystallization events. Both releasability and transcriptability are of tremendous importance for PGM process of ChGs. However, the moldability of ChG has thus far been evaluated mainly based on the trial-and-error approaches. In this respect, Lee *et al.* [85] proposed more systematic and intuitive screening guidelines using unempirical indicators that can be numerically derived from the structural characteristics of ChGs. In this work adopting Ge-Sb-Se glasses, four primary criteria have emerged for compositional screening. First, the off-stoichiometry quantified by the S-parameter can be useful to avoid Se-rich compositions that are more prone to volatility and thermal degradation due to presence of weaker Se-Se bonds. Second, the mean coordination number (MCM) serves as a topological indicator of the network rigidity. Optimal moldable compositions fall within the MCM range of 2.6–2.7, which aligns with the structural threshold of 2.67 for ChGs. Third, E_{ave} reflects the thermal stability of the glass network. Compositions with E_{ave} > 2.55 eV exhibit better thermal and mechanical

properties, thus being better compositions for PGM process. Lastly, crystallization tendency is inferred from the Ge-Se bond fraction, with values below 0.8 correlating with improved glass-forming ability and reduced devitrification risk during processing. These parameters which are derived from both experimental and theoretical considerations, are effective in compositional screening of moldable ChG compositions. Ternary Ge-Sb-Se glasses have been actively studied for use as LWIR lenses [71, 85–91], and together with those macroscopic properties the structural information on ChGs is valuable in assessing the process compatibility, as exemplified in the case of Ge-Sb-Se glasses.

6 Summary

As one of the traditional ceramic substances, glass can thrive more vigorously in its traditional application sectors in the form of flat glass and container glass by embracing more functionalities. The most advanced display modules and semiconductor chips are currently manufactured mostly in East Asia. This geographic imbalance provides unique opportunities and challenges for the glass industry and for academia. Newly arising applications such as ultra-thin glass for flexible display modules and glass core substrate for semiconductor packaging will present unprecedented functionalities and benefits to glass materials.

The four topics sorted out of tons of research activities driven by South Korean universities addressed in this study are summarized in terms of current status and short-term outlook as follows.

1) The CALPHAD thermodynamic database for glass system and glassmaking process has been actively developed to assist glass research and the manufacturing process. In addition, a multi-component diffusion model for glass systems is being actively studied for various kinetic simulations. Recent research focuses on the expansion of the database to address key issues relevant to the decarbonization of the glassmaking process such as water solubility in glass, new redox agents, refractory wear in glass melting furnace, and electrode materials for an electric melting furnace. However, the limited availability of phase diagram and thermodynamic data pose challenging issues for the database development relevant to the decarbonization process.

2) In order to meet the demands for advanced glass lubricants for continuous casting of steel, investigations of structural understandings and their effects on non-Newtonian rheology, thermal properties, and glass forming ability are being actively pursued. In particular, application of MAE and Mie scattering is believed to be an effective design principle to enhance lubrication without deteriorating heat transfer controlling ability. In consideration of the necessity of increasing scrap recycling to achieve carbon neutrality during steel manufacturing, further investigations should be done on rheological behavior of supercooled silicate glass lubricant melts in order to mitigate the cracking on continuously cast steels with a greater number of accumulated impurities.

3) Quantum dots and perovskite nanocrystals are still widely studied for next generation color converters or phosphoric materials for high picture quality displays including micro-LED display and anti-counterfeit applications, thus offering high chances for robust quantum dot or perovskite nanocrystal embedded glasses. However, (1) sub-micron sized glass powders with stable PL-QY, (2) Pb-free perovskite nanocrystals and (3) glass materials for direct driving LED remain as challenging issues for their future applications.

4) The thermal imaging market is supposed to steadily expand with a conspicuously steep inflection arising in the automobile industry caused by the regulations mandating employment of the AEB system. It is noteworthy that the cost of LWIR image sensors based on microbolometer arrays is decreasing rapidly to meet the demands of the automotive industry, and in this regard a group of well-qualified chalcogenide glasses will be promising as molded lenses for the high-resolution thermal cameras. In particular, those chalcogenide glasses consisting of environmentally less harmful and relatively cheaper constituents would be preferred in the civilian sectors.

References:

[1] SEOK B C, JUNG J P. Recent progress of TGV technology for high performance semiconductor packaging[J]. J Weld Join, 2024, 42(2): 155–164.

[2] LEE J I, KO S Y, CHOI Y G. Chemical strengthening of ultra-thin

glass for use as cover window of flexible displays[J]. Ceramist, 2022, 25(3): 287–298.

[3] SAUNDERS N, MIODOWNIK A P. CALPHAD: Calculation of Phase Diagrams - A Comprehensive Guide[M]. Amsterdam: Elsevier, 1998

[4] SPENCER P J. A brief history of CALPHAD[J]. Calphad, 2008, 32(1): 1–8.

[5] JUNG I H. Overview of the applications of thermodynamic databases to steelmaking processes[J]. Calphad, 2010, 34(3): 332–362.

[6] JUNG I H, VAN ENDE M A. Computational thermodynamic calculations: FactSage from CALPHAD thermodynamic database to virtual process simulation[J]. Metall Mater Trans B, 2020, 51(5): 1851–1874.

[7] JUNG I H. Thermodynamic packages and databases[M]//Treatise on Process Metallurgy. Amsterdam: Elsevier, 2024: 513–518.

[8] BALE C W, BÉLISLE E, CHARTRAND P, et al. FactSage thermochemical software and databases, 2010–2016[J]. Calphad, 2016, 54: 35–53.

[9] PELTON A D, DEGTEROV S A, ERIKSSON G, et al. The modified quasichemical model I: Binary solutions[J]. Metall Mater Trans B, 2000, 31(4): 651–659.

[10] PELTON A D, CHARTRAND P. The modified quasi-chemical model: Part II. Multicomponent solutions[J]. Metall Mater Trans A, 2001, 32(6): 1355–1360.

[11] HILLERT M. The compound energy formalism[J]. J Alloys Compd, 2001, 320(2): 161–176.

[12] KWON S Y. Thermodynamic optimization of ZrO_2-containing systems in the CaO–MgO–SiO_2–Al_2O_3–ZrO_2 system[D]. Quebec, Canada: McGill University, 2015.

[13] LEE J, KWON S Y, JUNG I H. Phase diagram study and thermodynamic assessment of the Na_2O-ZrO_2 system[J]. J Eur Ceram Soc, 2021, 41(15): 7946–7956.

[14] LEE J, YIN T T, HUDON P, et al. Phase diagram study of the SnO_2-SiO_2 system and thermodynamic optimization of the SnO-SnO_2-SiO_2 system[J]. Ceram Int, 2022, 48(3): 4141–4152.

[15] YIN T. Coupled thermodynamic modeling and experimental study of the SnO_2–SnO–CaO–SiO_2 system[D]. Quebec, Canada: McGill University, 2018.

[16] YIN T T, LEE J, MOOSAVI-KHOONSARI E, et al. Critical evaluation and the thermodynamic optimization of the Sn-O system[J]. Ceram Int, 2021, 47(20): 29267–29276.

[17] RAHMAN M, HUDON P, JUNG I H. A coupled experimental study and thermodynamic modeling of the SiO_2-P_2O_5 system[J]. Metall Mater Trans B, 2013, 44(4): 837–852.

[18] KIM D G, VAN ENDE M A, HUDON P, et al. Coupled experimental study and thermodynamic optimization of the K_2O-SiO_2 system[J]. J Non Cryst Solids, 2017, 471: 51–64.

[19] KIM M K, JUNG I H. Coupled phase diagram study and thermodynamic modeling of the Na_2O-B_2O_3-ZnO system[J]. J Eur Ceram Soc, 2024, 44(12): 7370–7382.

[20] KONAR B, HUDON P, JUNG I H. Experimental investigation of the $LiAlSi_2O_6$-$MgSiO_3$ and $LiAlSi_2O_6$-$CaMgSi_2O_6$ isopleths at 1 atm[J]. J Am Ceram Soc, 2017, 100(7): 3269–3282.

[21] KONAR B, KIM D G, JUNG I H. Critical thermodynamic optimization of the Li_2O-Al_2O_3-SiO_2 system and its application for the thermodynamic analysis of the glass-ceramics[J]. J Eur Ceram Soc, 2018, 38(11): 3881–3904.

[22] JUNG I H. Thermodynamic modeling of gas solubility in molten slags (II): Water[J]. ISIJ Int, 2006, 46(11): 1587–1593.

[23] GRUNDY A N, LIU H, JUNG I H, et al. A model to calculate the viscosity of silicate melts: Part I: Viscosity of binary SiO_2-MeO_x systems (Me = Na, K, Ca, Mg, Al)[J]. Int J Mater Res, 2008, 99(11): 1185–1194.

[24] GRUNDY A N, JUNG I H, PELTON A D, et al. A model to calculate the viscosity of silicate melts: Part II: The $NaO_{0.5}$–MgO–CaO–$AlO_{1.5}$–SiO_2 system[J]. Int J Mater Res, 2008, 99(11): 1195–1209.

[25] KIM W Y, PELTON A D, DECTEROV S A. A model to calculate the viscosity of silicate melts: Part III: Modification for melts containing alkali oxides[J]. Int J Mater Res, 2012, 103(3): 313–328.

[26] KWON S Y, HILL R J, JUNG I H. A model for multicomponent diffusion in oxide melts[J]. Calphad, 2021, 72: 102246.

[27] KWON S Y, HILL R J, JUNG I H. Multi-ion diffusion model and application to solid dissolution in CaO–Al_2O_3–SiO_2 melts[J]. J Am Ceram Soc, 2024, 107(3): 1835–1847.

[28] SHIN S H, CHO J W, KIM S H. Shear thinning behavior of calcium silicate-based mold fluxes at 1623 K[J]. J Am Ceram Soc, 2014, 97(10): 3263–3269.

[29] SHIN S H, CHO J W, KIM S H. Structural investigations of CaO–CaF_2–SiO_2–Si_3N_4 based glasses by Raman spectroscopy and XPS considering its application to continuous casting of steels[J]. Mater Des, 2015, 76: 1–8.

[30] SHIN S H, CHO J W, KIM S H. Controlling the shear thinning property of calcium silicate melts by addition of Si_3N_4[J]. J Non Cryst Solids, 2015, 423/424: 45–49.

[31] SHIN S H, YOON D W, CHO J W, et al. Controlling shear thinning property of lime silica based mold flux system with borate additive at 1623 K[J]. J Non Cryst Solids, 2015, 425: 83–90.

[32] SHIN S H, JEONG Y C, CHO J W, et al. Highlighting a rheological behavior of glass melt at high temperature[J]. J Non Cryst Solids, 2018, 499: 41–48.

[33] JEONG Y C, SHIN S H, BAEK J Y, et al. Influence of silicon carbide on shear-thinning behavior of CaO-SiO_2-CaF_2-based mold fluxes[J]. Metall Mater Trans B, 2021, 52(4): 2048–2055.

[34] LEE J H, YEO T M, CHO J W. Effect of Li_2O on melt crystallization of CaO–SiO_2–CaF_2 based glasses[J]. Ceram Int, 2021, 47(5): 6773–6778.

[35] YEO T M, CHO J W. Effect of Li_2O on non-isothermal crystallization of cuspidine in CaO–SiO_2–CaF_2 glasses[J]. Metall Mater Trans B, 2021, 52(4): 2186–2193.

[36] YEO T M, JEON J M, HYUN S H, et al. Effects of Li_2O on structure of CaO-SiO_2-CaF_2-Na_2O glasses and origin of crystallization delay[J]. J Mol Liq, 2022, 347: 117997.

[37] HYUN S H, YEO T M, HA H M, et al. Structural evidence of mixed alkali effect for aluminoborosilicate glasses[J]. J Mol Liq, 2022, 347: 118319.

[38] YEO T M, CHO J W, HUNG I, et al. Unraveling the mechanism of crystallization delay with Li_2O in CaO-SiO_2-CaF_2-B_2O_3-Na_2O melts[J]. J Am Ceram Soc, 2022, 105: 6140–6148.

[39] YEO T M, YUAN B, LOVI J, et al. Resolving the mixed-alkali effect on the viscoelastic behavior of supercooled liquids[J]. Acta Mater, 2023, 242: 118447.

[40] YEO T M, CHO J W, SEN S. Deciphering the Mixed-Alkali effect in supercooled oxide liquids: Results from dynamic and thermodynamic measurements[J]. Acta Mater, 2024, 269: 119798.

[41] CHO J W, BLAZEK K, FRAZEE M, et al. Assessment of CaO–Al_2O_3 based mold flux system for high aluminum TRIP casting[J]. ISIJ Int, 2013, 53(1): 62–70.

[42] SHI C B, SEO M D, CHO J W, et al. Crystallization characteristics of CaO-Al_2O_3-based mold flux and their effects on in-mold performance during high-aluminum TRIP steels continuous casting[J]. Metall Mater Trans B, 2014, 45(3): 1081–1097.

[43] YOON D W, CHO J W, KIM S H. Assessment of heat transfer through mold slag film considering radiative absorption behavior of mold fluxes[J]. Met Mater Int, 2015, 21(3): 580–587.

[44] YOON D W, CHO J W, KIM S H. Scattering effect of iron metallic particles on the extinction coefficient of CaO-SiO_2-B_2O_3-Na_2O-Fe_2O_3-CaF_2 glasses[J]. Metall Mater Trans B, 2016, 47(5): 2785–2792.

[45] YOON D W, CHO J W, KIM S H. Controlling radiative heat transfer across the mold flux layer by the scattering effect of the borosilicate mold flux system with metallic iron[J]. Metall Mater Trans B, 2017, 48(4): 1951–1961.

[46] HYUN S H, CHO J W. Heat transfer control by dispersed metallic particles in glassy mold flux film for continuous steel casting[J]. J Am Ceram Soc, 2020, 103(10): 5678–5687.

[47] CHUNG W J, NAM Y H. Review: A review on phosphor in glass as a high power LED color converter[J]. ECS J Solid State Sci Technol, 2020, 9(1): 016010.

[48] LEE Y K, LEE J S, HEO J, et al. Phosphor in glasses with Pb-free silicate glass powders as robust color-converting materials for white LED applications[J]. Opt Lett, 2012, 37(15): 3276–3278.

[49] KIM K H, CHOI Y G, IM W B, et al. Rare earth dependent formation of PbF_2 nanocrystals and its effect on the emission properties in oxyfluoride glasses[J]. Met Mater Int, 2013, 19(2): 347–352.

[50] BAE S R, CHOI Y G, IM W B, et al. Rare earth doped silicate-oxyfluoride glass ceramics incorporating LaF_3 nano-crystals for UV-LED color conversion[J]. Opt Mater, 2013, 35(11): 2034–2038.

[51] LEE S H, BAE S R, CHOI Y G, et al. Eu^{2+}/Eu^{3+}-doped oxyfluoride glass ceramics with LaF_3 for white LED color conversion[J]. Opt Mater, 2015, 41: 71–74.

[52] LEE S H, BAE S R, CHOI Y G, et al. Visible spectroscopic properties of SiO_2–Na_2O–Al_2O_3–LaF_3 glass ceramics doped with Dy^{3+} and Ho^{3+} under blue LED excitation[J]. J Non Cryst Solids, 2016, 431: 126–129.

[53] LEE H, LEE S H, CHOI Y G, et al. Eu^{2+} and Mn^{2+} Co-doped oxyfluoride glass ceramic for white color conversion of 400 nm UV-LED[J]. J Lumin, 2020, 222: 117156.

[54] LEE H, CHUNG W J. Eu^{2+}-doped oxyfluoride glass-ceramic with nepheline as an efficient 400 nm UV-LED color converter[J]. J Am Ceram Soc, 2021, 104(8): 4024–4032.

[55] LEE H, CHUNG W J, IM W B. Pr^{3+}-doped oxyfluoride glass ceramic as a white LED color converter wide color gamut[J]. J Lumin, 2021, 236: 118064.

[56] LEE H, LEE J J, SHINOZAKI K, et al. Eu^{3+}-Tb^{3+}-Tm^{3+} co-doped oxyfluoride glass with high quantum yield for a robust white LED color converter[J]. Opt Mater, 2022, 132: 112882.

[57] HAN K, YOON S, CHUNG W J. CdS and CdSe quantum dot-embedded silicate glasses for LED color converter[J]. Int J Appl Glass Sci, 2015, 6(2): 103–108.

[58] HAN K, IM W B, HEO J, et al. A complete inorganic colour converter based on quantum-dot-embedded silicate glasses for white light-emitting-diodes[J]. Chem Commun, 2016, 52(17): 3564–3567.

[59] HAN K, IM W B, HEO J, et al. Compositional dependency of Cd-S-Se quantum dots within silicate glass on color conversion for a white LED[J]. J Am Ceram Soc, 2019, 102(4): 1703–1709.

[60] HAN K, HEO J, CHUNG W J. The effect of rare earth on color conversion properties of Cd–S–Se quantum dot embedded silicate glasses for white LED[J]. Opt Mater, 2021, 111: 110545.

[61] HAN K, NAM Y H, KIM S H, et al. The formation mechanism of Cd–S–Se quantum dots with CdSe/CdS core–shell structure within silicate glass[J]. J Am Ceram Soc, 2023, 106(11): 6500–6509.

[62] HAN K, HEO J, IM W B, et al. Cd–S–Se quantum dot embedded glasses with dual emissions for wide color gamut white LED[J]. Int J Appl Glass Sci, 2021, 12(3): 415–423.

[63] PHAM T T, LEE H, LEE J J, et al. Perovskite nanocrystal-embedded glasses for photonic applications[J]. J Korean Ceram Soc, 2022, 59(6): 749–762.

[64] NAM Y H, HAN K, CHUNG W J, et al. Double encapsulation of $CsPbBr_3$ perovskite nanocrystals with inorganic glasses for robust color converters with wide color gamut[J]. ACS Appl Nano Mater, 2021, 4(7): 7072–7078.

[65] LEE J J, LEE H, KIM U, et al. Flexible remote phosphor color converter based on ultra-thin glass and $CsPbBr_3$ perovskite nanocrystal-embedded glass for a wide-color-gamut white LED[J]. J Mater Chem C, 2023, 11(3): 898–902.

[66] LEE H, GELIJA D, KIM U, et al. Compositional study of borosilicate $CsPbBr_3$ perovskite nanocrystals embedded glass for chemically stable white LEDs[J]. J Korean Ceram Soc, 2024, 61(3): 482–491.

[67] PHAM T T, LEE J J, GELIJA D, et al. Effect of Al_2O_3 and Ga_2O_3 on the photoluminescence of borosilicate glasses embedding $CsPbBr_3$ perovskite nanocrystals[J]. Int J Appl Glass Sci, 2025, 16(4): e16709.

[68] GELIJA D, KIM H A, CHUNG W J. $CsPbBr_3$ perovskite nanocrystals embedded in boro-silicate glasses doped with Pr_2O_3 for green color converters[J]. Opt Mater, 2025, 167: 117251.

[69] LEE J J, GELIJA D, KIM H A, et al. Red color converting $CsPb(Br/I)_3$ perovskite nano-crystals within germanate glasses for wide color gamut display applications[J]. Ceram Int, 2024, 50(23): 50327–50336.

[70] CHOI Y G, HEO J. 1.3 μm emission and multiphonon relaxation phenomena in PbO–Bi_2O_3–Ga_2O_3 glasses doped with rare-earths[J]. J Non Cryst Solids, 1997, 217(2–3): 199–207.

[71] LEE J H, LEE W H, PARK J K, et al. Thermal properties of ternary Ge–Sb–Se chalcogenide glass for use in molded lens applications[J]. J Non Cryst Solids, 2016, 431: 41–46.

[72] KIM H, YOON I J, CHOI Y G. Adjustment of refractive index of Ge-Ga-Se glass *via* Te addition for infrared-imaging applications[J]. J Non Cryst Solids X, 2023, 18: 100190.

[73] LIU C. Exploring the potential of chalcogenide lens designs for cost-effective LWIR systems[J]. EPJ Web Conf, 2024, 309: 03011.

[74] LI J. Automotive Infrared Camera Technologies: Markets for Seeing Inside and Outside the Vehicle[EB/OL]. [2024–10–07]. https://www.idtechex.com/en/webinar/automotive-infrared-camera-technologies-markets-for-seeing-inside-and-outside-the-vehicle/616.

[75] FEIN H, PONTING M. SWaP advantage of replacing high performance glass achromatic doublet with a polymeric nanolayer GRIN achromatic singlet[C]//Advanced Optics for Defense Applications: UV through LWIR III. Orlando, USA. SPIE, 2018: 10.

[76] RAMSEY J L, LINDBERG G P, CAMPBELL R, et al. Experimental verification of a MWIR/LWIR 3x continuous zoom lens (Rising Researcher Paper)[C]//Advanced Optics for Imaging Applications: UV through LWIR IV. Baltimore, USA. SPIE, 2019: 24.

[77] TEPEGOZ M, KUCUKKOMURLER A, TANKUT F, et al. A miniature low-cost LWIR camera with a 160 × 120 microbolometer FPA[J]. Infrared Technol Appl XL, 2014, 9070: 90701O.
[78] LEE J H, KIM H, CHOI Y G. Compositional optimization of chalcogenide glasses for use as imaging lenses in the long-wavelength infrared range[J]. Ceramist, 2020, 23(3): 286–301.
[79] MATSUSHITA Y, TOMITA M, SATO F, et al. Infrared optical elements using unique chalcogenide glass materials[C]//Terahertz, RF, Millimeter, and Submillimeter-Wave Technology and Applications XVIII. San Francisco, USA. SPIE, 2025: 51.
[80] LEE J H, LEE W H, CHOI J H, et al. High refractive index dispersion of compositionally optimized Ge-Ga-Sb-S sulfide glass for use as molded lens in the long-wavelength infrared range[J]. Ceram Int, 2018, 44(17): 21956–21961.
[81] LEE J H, CHOI J H, YI J H, et al. Unravelling interrelations between chemical composition and refractive index dispersion of infrared-transmitting chalcogenide glasses[J]. Sci Rep, 2018, 8(1): 15482.
[82] LEE J H, KIM H, LEE J I, et al. Infrared transmission and refractive index dispersion of mixed chalcogen Ge-Sb-S-Se glasses for use in molded lens applications[J]. J Non Cryst Solids, 2020, 546: 120258.
[83] KIM H, LEE J H, LEE J I, et al. Compositional dependence of infrared transmission in Ge-based chalcogenide glasses[J]. Phys Status Solidi B, 2020, 257(11): 2000164.
[84] BLANC W, CHOI Y G, ZHANG X H, et al. The past, present and future of photonic glasses: A review in homage to the United Nations International Year of glass 2022[J]. Prog Mater Sci, 2023, 134: 101084.
[85] LEE J H, KIM H, CHOI Y G. Compositional screening of chalcogenide glass for use as molded lens: An exemplary case of ternary Ge-Sb-Se glass[J]. J Asian Ceram Soc, 2020, 8(4): 971–983.
[86] PARK J K, LEE J H, SHIN S Y, et al. Compositional dependence of hardness of Ge-Sb-Se glass for molded lens applications[J]. Arch Metall Mater, 2015, 60(2): 1205–1208.
[87] LEE W H, YI J H, LEE J H, et al. Thermal expansion behavior of Ge-Sb-Se glasses in a compositional range for molded infrared lens applications[J]. Int J Appl Glass Sci, 2017, 8(2): 226–232.
[88] LEE J H, YI J H, LEE W H, et al. Crystallization behavior of Ge-Sb-Se glasses in the compositional range for use as molded lenses[J]. J Non Cryst Solids, 2018, 481: 21–26.
[89] LEE J H, KIM H, LEE W H, et al. Surface modification of chalcogenide glass for diamond-like-carbon coating[J]. Appl Surf Sci, 2019, 478: 802–805.
[90] LEE J H, KIM H, YOON I J, et al. Influence of oxygen incorporation on infrared transmission of ternary Ge-Sb-Se chalcogenide glass in the compositional range for use in infrared-imaging applications[J]. Ceram Int, 2021, 47(24): 34633–34638.
[91] LEE J H, KIM H, YOON I J, et al. Reassessing the average bond energy of Ge-based chalcogenide glasses[J]. J Non Cyrst Solids, 2022, 590: 121702.

作者贡献声明：

YOON Il Jung, LEE Jae sung：绘制图表，撰写稿件；

JUNG In-Ho, CHUNG Woon Jin, CHO Jung-Wook, CHOI Yong Gyu：提出研究方向，设计论文框架，修订稿件。

Recent Progresses in Application-Oriented Glass Research in South Korea

YOON Il Jung[1], *LEE Jae sung*[2], *JUNG In-Ho*[2,3], *CHUNG Woon Jin*[4], *CHO Jung-Wook*[5], *CHOI Yong Gyu*[1]

(1. Department of Materials Science and Engineering, Korea Aerospace University, Goyang 10540, South Korea; 2. Department of Materials Science and Engineering, Seoul National University, Seoul 08826, South Korea; 3. Research Institute of Advanced Materials (RIAM), Seoul National University, Seoul 08826, South Korea; 4. Division of Advanced Materials Engineering, Kongju National University, Cheonan 31080, South Korea; 5. Graduate Institute of Ferrous & Eco Materials Technology, Pohang University of Science and Technology (POSTECH), Pohang 37673, South Korea)

Extended Abstract

Abstract The downstream glass industry in South Korea exhibits a distinctive structure compared with that of other non-Asian countries, as its semiconductor and display sectors are tightly integrated with the glass materials supply chain. In this review, the distinct features of glass-related industrial research and development in South Korea are addressed by taking two representative applications of glasses, *i.e.*, glass core substrate for semiconductor packaging applications and ultra-thin glass for use as cover window of flexible display modules. In the case of glass core substrate and glass interposer, the inherent brittleness of glassy materials imposes constraints across the process flow, requiring precise control over laser irradiation, chemical etching, redistribution layer formation, and singulation. Ultra-thin glass needs to be durable during repeated deformations, so that its thickness is typically on the order of several tens of micrometers. At such thickness levels, resistance to mechanical deformations becomes a primary concern, and therefore processing steps from cutting, chamfering, and healing to chemical strengthening play a decisive role in determining mechanical reliability and optical clarity of ultra-thin glass. Flexible display devices with other form factors featuring multi-foldable, slidable or rollable capability would be realized along with advancement of processing technologies associated with ultra-thin glass.

With an emphasis on the application-oriented research activities directly or indirectly related to glass materials led by South Korean universities, four different topics are introduced in this review: 1) a thermodynamic database for glass-forming systems, 2) mold flux systems used in steel casting, 3) glasses doped with quantum dots and/or perovskite nano-crystals, and 4) chalcogenide glasses for thermal imaging. For each topic, recent advances are described in conjunction with their basic concepts and future perspectives. The CALPHAD (CALculation of PHAse Diagrams) thermodynamic database for glass-forming system and glassmaking process has been actively developed to assist glass research and the manufacturing process. In addition, a multi-component diffusion

model for glass systems is being actively studied for various kinetic simulations. Recent research focuses on the expansion of the database to address key issues relevant to the decarbonization of the glassmaking process such as water solubility in glass, new redox agents, refractory wear in glass melting furnace, and electrode materials for an electric melting furnace. However, the limited availability of phase diagram and thermodynamic data pose challenging issues for the database development relevant to the decarbonization process.

In order to meet the demands for advanced glass lubricants for continuous casting of steel, investigations of structural understandings and their effects on non-Newtonian rheology, thermal properties, and glass forming ability are being actively pursued. In particular, application of mixed alkali effect and Mie scattering is believed to be an effective design principle to enhance lubrication without deteriorating heat transfer controlling ability. In consideration of the necessity of increasing scrap recycling to achieve carbon neutrality during steel manufacturing, further investigations should be done on rheological behavior of supercooled silicate glass lubricant melts in order to mitigate the cracking on continuously cast steels with a greater number of accumulated impurities.

Quantum dots and perovskite nanocrystals are still widely studied for next generation color converters or phosphoric materials for high picture quality displays including micro-LED display and anti-counterfeit applications, thus offering high chances for robust quantum dot or perovskite nanocrystal embedded glasses. However, several issues such as sub-micron sized glass powders with stable PL-QY, Pb-free perovskite nanocrystals, and glass materials for direct driving LED remain as challenging issues for their future applications.

The thermal imaging market is expected to steadily expand with a conspicuously steep inflection arising in the automobile industry caused by the regulations mandating employment of the autonomous emergence braking system. It is noteworthy that the cost of LWIR image sensors based on microbolometer arrays is decreasing rapidly to meet the demands of the automotive industry, and in this regard a group of well-qualified chalcogenide glasses will be promising as molded lenses for the high-resolution thermal cameras. Specifically, those chalcogenide glasses consisting of environmentally less harmful and relatively cheaper constituents would be preferred in the civilian sectors.

Summary and Prospects Across diverse application domains, glass materials are engineered to meet increasingly stringent criteria with regard to performance, reliability, and sustainability. It is worth mentioning that the most advanced display modules and semiconductor chips are currently manufactured mostly in East Asia. This geographic imbalance provides unique opportunities and challenges for both of the glass industry and academia. New applications such as ultra-thin glass for flexible display modules and glass core substrate for semiconductor packaging will present unprecedented functionalities and benefits to glass materials.

Keywords ultra-thin glass; glass core substrate; CALPHAD thermodynamic database; mold flux; quantum dot and perovskite glass; chalcogenide glass